

ARMY RESEARCH LABORATORY



Thermophotovoltaic Energy Conversion for Personal Power Sources

by C. Mike Waits

ARL-TR-5942

February 2012

NOTICES

Disclaimers

The findings in this report are not to be construed as an official Department of the Army position unless so designated by other authorized documents.

Citation of manufacturer's or trade names does not constitute an official endorsement or approval of the use thereof.

Destroy this report when it is no longer needed. Do not return it to the originator.

Army Research Laboratory

Adelphi, MD 20783-1197

ARL-TR-5942

February 2012

Thermophotovoltaic Energy Conversion for Personal Power Sources

C. Mike Waits

Sensors and Electron Devices Directorate, ARL

REPORT DOCUMENTATION PAGE			Form Approved OMB No. 0704-0188		
Public reporting burden for this collection of information is estimated to average 1 hour per response, including the time for reviewing instructions, searching existing data sources, gathering and maintaining the data needed, and completing and reviewing the collection information. Send comments regarding this burden estimate or any other aspect of this collection of information, including suggestions for reducing the burden, to Department of Defense, Washington Headquarters Services, Directorate for Information Operations and Reports (0704-0188), 1215 Jefferson Davis Highway, Suite 1204, Arlington, VA 22202-4302. Respondents should be aware that notwithstanding any other provision of law, no person shall be subject to any penalty for failing to comply with a collection of information if it does not display a currently valid OMB control number. PLEASE DO NOT RETURN YOUR FORM TO THE ABOVE ADDRESS.					
1. REPORT DATE (DD-MM-YYYY) February 2012		2. REPORT TYPE Final		3. DATES COVERED (From - To) November 2010 to September 2011	
4. TITLE AND SUBTITLE Thermophotovoltaic Energy Conversion for Personal Power Sources			5a. CONTRACT NUMBER		
			5b. GRANT NUMBER		
			5c. PROGRAM ELEMENT NUMBER		
6. AUTHOR(S) C. Mike Waits			5d. PROJECT NUMBER		
			5e. TASK NUMBER		
			5f. WORK UNIT NUMBER		
7. PERFORMING ORGANIZATION NAME(S) AND ADDRESS(ES) U.S. Army Research Laboratory ATTN: RDRL-SED-E 2800 Powder Mill Road Adelphi, MD 20783-1197			8. PERFORMING ORGANIZATION REPORT NUMBER ARL-TR-5942		
9. SPONSORING/MONITORING AGENCY NAME(S) AND ADDRESS(ES)			10. SPONSOR/MONITOR'S ACRONYM(S)		
			11. SPONSOR/MONITOR'S REPORT NUMBER(S)		
12. DISTRIBUTION/AVAILABILITY STATEMENT Approved for public release; distribution unlimited.					
13. SUPPLEMENTARY NOTES					
14. ABSTRACT Advancements in photovoltaic, thermal emission, and compact liquid fueled combustion sources enable thermophotovoltaic energy conversion to compete with battery and fuel technology for compact power applications. This report highlights all components of the thermal-to-electric energy conversion (TEC) system including the balance-of-plant and provides a review of the state of the art. Evaluation of each component's performance determined that a 10% efficient thermophotovoltaic power source could be realizable by integrating state-of-the art components. Reduction of the photovoltaic cell bandgap and Auger recombination, combined with emitters using photonic crystals to tailor the emission spectrum and heat recuperation within a combustion-based heat source, can lead to TEC efficiencies greater than 20% with temperatures below 1000 °C. Such a power source could have an energy density reaching 1000 W·h/kg and power densities in the 10's W/kg with a multi-fuel capability offering a tremendous advancement from today's battery technology.					
15. SUBJECT TERMS Thermophotovoltaics, photovoltaic cell, microburner, catalytic combusting, emitter					
16. SECURITY CLASSIFICATION OF:			17. LIMITATION OF ABSTRACT UU	18. NUMBER OF PAGES 38	19a. NAME OF RESPONSIBLE PERSON Christopher M. Waits
a. REPORT Unclassified	b. ABSTRACT Unclassified	c. THIS PAGE Unclassified			19b. TELEPHONE NUMBER (Include area code) (301) 394-0057

Contents

List of Figures	iv
List of Tables	iv
1. Introduction	1
2. Thermophotovoltaic Energy Conversion	3
2.1 Thermophotovoltaic Overview.....	3
2.2 Blackbody Emitter.....	4
2.3 Photovoltaic Cells in Thermophotovoltaic.....	5
2.4 Spectral Tuning	7
2.5 Thermophotovoltaic and Thermoelectric Conversion Efficiency Comparison	11
2.6 Thermophotovoltaic Technology Discussion.....	15
2.6.1 Thermophotovoltaic Packaging and Practical Considerations.....	15
2.6.2 Heat Exchanger	15
2.6.3 Future High Power Density Thermophotovoltaic Strategies	16
3. TEC System	16
3.1 Heat Source	18
3.2 Balance-of-plant Components.....	19
3.3 TEC System Power Density and Conversion.....	20
4. Conclusions	23
5. References	24
List of Symbols, Abbreviations, and Acronyms	29
Distribution List	30

List of Figures

Figure 1. Primary components of thermophotovoltaic energy converter.	3
Figure 2. Example blackbody spectra from equation 2 for temperatures of 500, 750, and 1000 °C.	4
Figure 3. Example cut-off wavelength for a 0.6-eV bandgap.....	6
Figure 4. Maximum spectral efficiency from reference 17.	8
Figure 5. The power density of a notional thermophotovoltaic system is plotted vs. emitter temperature. A photovoltaic cell efficiency of 30% is used in the calculation of the power density.	10
Figure 6. Thermophotovoltaic energy conversion efficiency for example bandgap energies assuming 30% photovoltaic conversion of in-band radiation and R-values ranging from 0.05 to 0.10 giving rise to the thickness of the curves.....	10
Figure 7. Thermoelectric conversion efficiency is plotted vs. the temperature of the hot side with a cold side temperature at 27 °C.	13
Figure 8. Thermophotovoltaic and thermoelectric conversion efficiency plotted vs. temperature. 14	
Figure 9. Plot showing the view factor of equal squares vs. the ratio of the square length to the spacing.	14
Figure 10. Ragonne plot for TEC assuming 10% conversion efficiency and assuming fuel storage is 10% of fuel weight for JP-8 fuel.....	21
Figure 11. Power density plotted vs. TEC conversion efficiency for durations of 24 and 72 h. Li-ion (dashed line) and Li-Air (dotted line) battery technologies are plotted for comparison. 22	
Figure 12. Energy plotted vs. TEC conversion efficiency for duration of 24 and 72 h. Li-ion (dashed line) and Li-Air (dotted line) battery technologies are plotted for comparison.	22

List of Tables

Table 1. Characteristics of candidate fuels (37).....	18
---	----

1. Introduction

Compact power sources having high energy and power densities are critical for numerous commercial and military applications. These applications can span from personal power sources for expeditions requiring long periods of time away from a power grid to unmanned air vehicles (UAVs) requiring only a few hours of running time. A power technology gap currently exists in the range of 10–100 W+ that is only spanned by battery technology because improvements in rechargeable batteries have not kept up with the power demand of new personal devices. High energy dense technologies are sought after to augment batteries and extend the available energy density well beyond state-of-the-art battery technology (140 W·h/kg for rechargeable lithium [Li]-ion technology [1]).

There is a focus in the military to develop power technologies that capitalize on the large energy content offered by hydrocarbons or alcohols. Modest conversion efficiencies of only a few percent can provide comparable energy density to battery technology with the added capability of instant recharge. Fuel cells have seen a lot of focus at all power levels and have become a promising technology to span the power technology gap. For example, Los Alamos National Laboratories developed a direct methanol fuel cell (DMFC) useful for personal power applications, which demonstrated an energy density of 550 W·h/kg for a 72-h mission duration and delivering 20 W of average electrical power with an overall efficiency of 33% (2). Smart Fuel Cell offers a 250-W DMFC suitable, for example, in UAV applications having approximately 464 W·h/kg (31.1 kWh in fuel cartridge and a 67-kg system weight with fuel) (3). Smart Fuel cell also offers Energy for You (EFOY) DMFCs on their Web site, claiming 721 W·h/kg for a 40-W average electrical power using their M10 cartridge (4). Although fuel cells continue to be improved and can have higher energy densities than batteries, there is a lack of fuel flexibility. For some applications, a mainstream fuel source such as propane, butane, gasoline, or diesel may be better options than hydrogen sources or methanol cartridges. Hydrogen fuels require engineered storage of hydrogen as a liquid or operate through the chemical release from hydrates, which currently prevent their use. Meanwhile, methanol has lower energy content than the longer chain alcohols and hydrocarbons.

Conversion of the chemical energy content of a fuel to electrical energy can be both efficient and fuel flexible by first converting the energy into heat. Electrical power converted from heat using a large temperature difference can efficiently extract the energy content and follows the Carnot efficiency. Such energy conversion has been accomplished through mechanical engines that convert chemical to mechanical through combustion and then mechanical to electrical using, for example, magnetic generators. Although mechanical heat engines are the mainstay at the large scale, there are significant challenges that exist when scaling engines below the kW level due to the increasing frictional losses and thermal management issues (6–8). Direct thermal-to-

electrical conversion (TEC) is another approach to achieve high efficiencies for compact platforms that has no moving parts within the core converter. Without moving components, the converter does not have scaling issues related to contact mechanics. Additionally, TEC can use external combustion as a heat source and thus can be more flexible than internal combustion engines, especially in the choice of fuel.

Three methods for continuous TEC have been studied significantly: (1) thermoelectric; (2) thermophotovoltaic; and (3) thermionic. The thermoelectric effect generates charge carriers from a temperature difference across the material and is used extensively by the National Aeronautics and Space Administration (NASA) for missions without access to solar energy. Thermophotovoltaic relies on converting thermal radiation via photovoltaic conversion techniques and has been investigated as early as 1963 (9). Thermionic extracts electrons from a low-working potential metallic surface across a small distance and high enough temperatures. Thermionic, like thermoelectric, is used in space applications where solar energy is not available (10, 11). Both thermophotovoltaic and thermionic traditionally require high temperature operation ($>1000\text{ }^{\circ}\text{C}$) and therefore no commercial products are available for compact power generation due to temperature stability issues. Thermoelectric has seen large growth with commercial products available due to having modest conversion efficiencies at lower temperatures as well as applications in cooling. Both thermoelectric cooling modules and generator modules are commercially available products. However, there has been limited success to develop a TEC system combined with a multi-fuel capable combustor for compact power generation using any of the three methods discussed.

Recent advances in low-bandgap photovoltaic cells and improved spectral control techniques have generated a renewed interest in thermophotovoltaic technology. Nelson and Guazzoni et al. (12, 13) provide an overview of the development of thermophotovoltaic technology for military applications and the limitations associated with high temperatures as of 2004. The advancements in photovoltaic cells and spectral control offer the potential for efficient conversion at operating temperatures considerably reduced from what was previously possible. The focus of this report is to provide a feasibility analysis of thermophotovoltaic as a compact power source and motivate future research efforts in this field. To accomplish this, this report provides the background with current state of the art identified when appropriate and identifies research areas to push this revitalized field. A comparison to thermoelectric conversion is made to provide a basis to a well understood technology. Finally, a comparison of thermal-to-electric conversion, which could be thermoelectric, thermionic, or thermophotovoltaic, is provided against battery technology, the only widely accepted power source to date.

2. Thermophotovoltaic Energy Conversion

2.1 Thermophotovoltaic Overview

Figure 1 describes the primary components of a thermophotovoltaic system: a heat source, an emitter, and a photovoltaic converter. The heat source supplies thermal energy to the emitter, which radiates the energy across a gap to a photovoltaic cell or an array of photovoltaic cells. The photovoltaic cell(s) then converts the thermal radiation to electrical energy, which can be delivered to a load or conditioning circuitry. Optical filters between the emitter and the photovoltaic cell, as well as reflectors deposited on the backside of the photovoltaic cell, are also common components (not included in figure 1). The optical cavity between the emitter and photovoltaic cell is often held under vacuum to minimize conduction and convective heat transfer. The TEC efficiency of a thermophotovoltaic converter at the device level is determined by the efficiency of each major component, namely,

$$\eta_{TEC} = \eta_{heat}\eta_{spectral}\eta_{cavity}\eta_{PV}, \quad (1)$$

where η_{heat} is the combined efficiency of the solar-to-heat or the chemical-to-heat conversion and the thermal efficiency of the heat delivered to the TEC (the emitter, in the case of the thermophotovoltaic), $\eta_{spectral}$ is how well the emitted spectrum can match the photovoltaic cell (discussed later), η_{cavity} is the fraction of the emitted radiation that reaches the surface of the photovoltaic cell, and η_{PV} is the photovoltaic conversion efficiency.

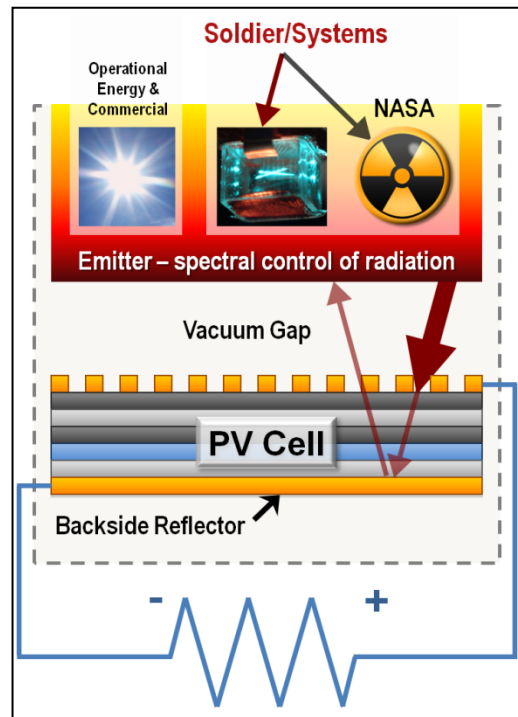


Figure 1. Primary components of thermophotovoltaic energy converter.

2.2 Blackbody Emitter

To elucidate the primary ideas behind optimizing thermophotovoltaic conversion for both efficiency and power, the emission from a blackbody source combined with a photovoltaic cell must be first described. Blackbody radiation within a medium having an index of refraction of n can be described by Planck's law:

$$e_b(\lambda, T) = n^2 \frac{2\pi hc_0}{\lambda^5 (e^{hc_0/kT} - 1)}, \quad (2)$$

where h is Planck's constant, c_0 is the speed of light in a vacuum, λ is the wavelength, k is Boltzmann's constant, and T is the temperature of the blackbody. Figure 2 illustrates two key characteristics of equation 2 with increasing temperature. Firstly, as temperature increases the amount of power, P , emitted per area, A , increases as

$$P/A = \int_0^\infty e_b(\lambda, T) d\lambda = \sigma_{sb} T^4 (W/m^2), \quad (3)$$

where σ_{sb} is the Stefan-Boltzmann constant. Equation 3 underscores the importance of temperature towards the total power available. For example, the power available from a blackbody held at temperatures of 500, 750, and 1000 °C are 2, 6.2, and 14.9 W/cm², respectively.

Secondly, the peak intensity shifts to lower wavelengths as the temperature is increased. This is important when considering the bandgap of the photovoltaic cell discussed in the following section. The peak wavelength at 500 °C is close to 3.9 μm while at 1000 °C is around 2.1 μm. Since only photons having wavelengths below the bandgap of the photovoltaic cell can be converted, the spectral dependence of the radiated power has a direct impact on the conversion efficiency.

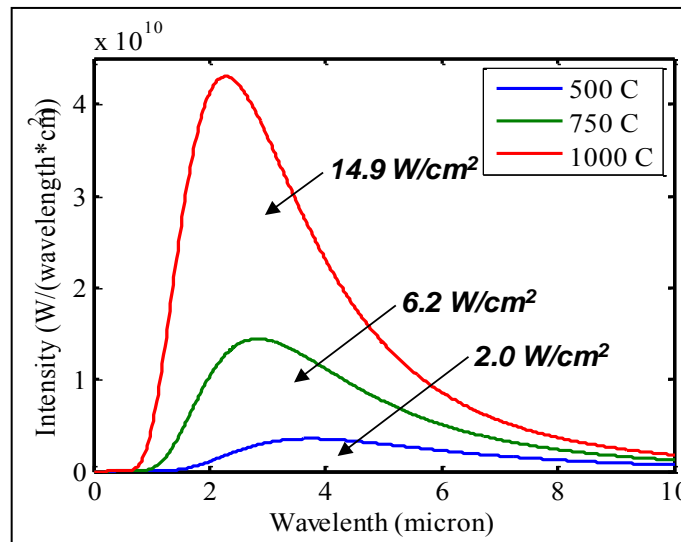


Figure 2. Example blackbody spectra from equation 2 for temperatures of 500, 750, and 1000 °C.

2.3 Photovoltaic Cells in Thermophotovoltaic

A photovoltaic cell is used to absorb the incident photon energy emanating from the emitter, convert it into charge carriers, and extract it to external circuitry loads with minimal loss. The dominant factors affecting the extraction of charge carriers are the minority carrier lifetimes (i.e., recombination losses) and carrier mobilities. The bandgap of the material system plays a key role in photon absorption. The bandgap should be small enough to effectively absorb the major part of the spectrum from equation 2. However, shorter wavelengths of the spectrum generate hot electron-hole pairs and most photon energy is lost as heat. Proper material selection and engineering of the cell structure is necessary to engineer the bandgap. The design of the thermophotovoltaic system must match the spectral properties of the emitter with the photovoltaic cell for optimal efficiency. The dependence on the spectral properties of the emitter is evident in the equation for the photovoltaic cell conversion efficiency, which can be written as (14)

$$\eta_{PV} = \frac{V_{OC}I_{SC}FF}{\text{Power In in-band}}, \quad (4)$$

where V_{OC} is the open-circuit voltage, I_{SC} is the short-circuit current, and FF is the fill factor for the photovoltaic cell. The numerator is the electrical power converted. The denominator is the amount of power delivered to the photovoltaic cell for energies above the photovoltaic cell bandgap.

Peak intensity of the radiated spectrum from relevant temperatures is well above that of the typical solar spectrum, thus the photovoltaic cells used in thermophotovoltaic conversion must be engineered from different material systems. Most common photovoltaic material systems for thermophotovoltaic conversion to date are gallium antimonide (GaSb)-related materials (homogeneous: 0.72 eV, indium gallium arsenide antimonide (InGaAsSb) on GaSb: 0.53 eV) or indium gallium arsenide (InGaAs) on an indium phosphide (InP) substrate (0.5 to 0.6 eV). The lower bandgap structures are achieved on the InP substrate using InP-based lattice-matched indium gallium arsenide phosphide (InGaAsP) and strained-compensated InGaAs/InGaAs quantum wells (15). Figure 3 demonstrates the amount of energy that is lost if a 0.6 eV bandgap photovoltaic cell is used. Comparing the total blackbody power density available in figure 2 to the power the photovoltaic is able to convert (below the bandgap wavelength) in figure 3, the maximum theoretical efficiency for a blackbody held at 1000 °C is 19% with a power density of 2.8 W/cm² and rapidly decreases with lower temperatures. Reducing the bandgap of the photovoltaic cell, for example, to 0.53 eV (i.e., InGaAsSb/GaSb cell), will increase the maximum theoretical efficiency for a blackbody held at 1000 °C to 27% and could have 4.0 W/cm² available for power conversion.

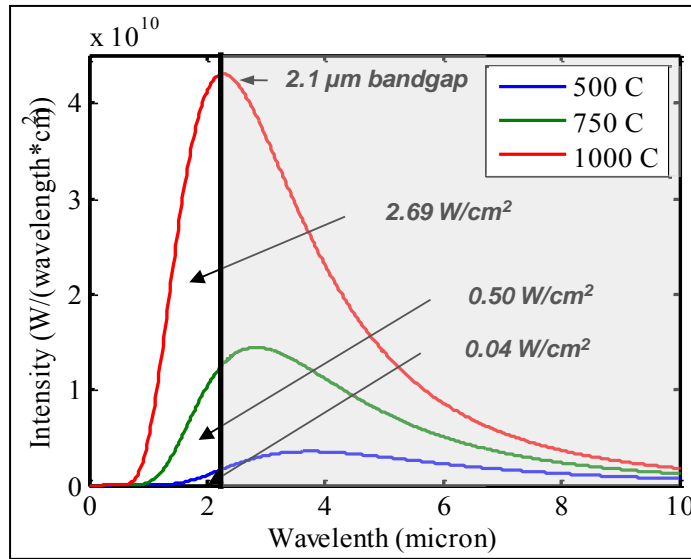


Figure 3. Example cut-off wavelength for a 0.6-eV bandgap.

There is a tradeoff between the photovoltaic cell conversion efficiency and the electronic bandgap of the selected material system. Lowering the bandgap requires new or modified material systems that have not had the same level of maturation as their solar cell counterparts and thus the current cell efficiencies are lower. For example, the 0.6-eV photovoltaic cells have demonstrated conversion efficiency around 24% while the 0.72-eV cells have demonstrated conversion efficiency closer to 30%. Although each can be further optimized to improve the efficiency, there is a fundamental limit to the efficiency associated with each material system and bandgap.

Numerous modeling efforts have determined the cell conversion will decrease with the bandgap due primarily to a reduced open-circuit voltage and is limited by both photon recycling and intrinsic Auger recombination. The optimal bandgap will depend on the received intensity. Tuley and Nicholas (16) discuss the spectral and photovoltaic cell conversion efficiency dependence on the bandgap. They predict the cell efficiencies and power densities using a model that includes Auger recombination, which they state becomes significant at lower bandgap energies and is comparable to radiative recombination at 0.60 eV. Dasheill et al., also suggests Auger recombination limits the open-circuit voltage and that it becomes dominant below 0.5 eV for the GaSb-based materials. For the InGaAs and InGaAsP material systems on InP both promising for 0.5 eV and up bandgap materials, Tuley and Nicholas predicts peak spectral and photovoltaic cell efficiency ($\eta_{\text{spectral}} * \eta_{\text{PV}}$) close to 23% for a gray-body source at 1200 K with an in-band emissivity of 1 and an out-of-band emissivity of 0.1.

New techniques to reduce Auger recombination are required to enable both high conversion efficiency and low-bandgap photovoltaic cells. This will allow both higher power density and higher TEC efficiency. In addition to improvements within the photovoltaic cell, the TEC efficiency can be improved for a given photovoltaic bandgap by eliminating or reducing the out-

of-band wavelengths emitted through spectral tuning. From the previous example of 23% conversion efficiency for a gray-body source at 1200 K, if the out-of-band emissivity can be reduced to 0.05, then the peak performance would occur close to 0.55 eV resulting in an efficiency increase predicted by Tuley and Nicholas to 28%.

2.4 Spectral Tuning

A blackbody or gray-body (i.e., a material having a constant emissivity <1) emission spectrum is not an ideal choice for a thermophotovoltaic system since a significant amount of the radiation has a wavelength above the photovoltaic bandgap wavelength. To maximize TEC efficiency only wavelengths below the bandgap wavelength of the photovoltaic cell should be emitted and thus the out-of-band wavelengths reduced or eliminated. This can be achieved through spectral tuning using an optical filter to reflect out-of-band wavelengths back to the emitter or a spectral emitter to only radiate in-band wavelengths.

Spectral tuning, however, often can diminish the in-band radiation since the in-band transmission of the optical filter is less than 100% and the in-band emissivity is less than 1 for the emitter. Diminished in-band radiation results in a reduction of the total power density. The total power emitted is a function of the emissivity of the material which can have a dependence on both wavelength and temperature:

$$Power = \int_0^{\infty} \epsilon(\lambda, T) e_b(\lambda, T) d\lambda. \quad (5)$$

There will be a tradeoff between power density and conversion efficiency when optimizing the thermophotovoltaic conversion system using spectral tuning.

Chubb devised a parameter, R , that indicates the level of spectral tuning by splitting up emissivity and reflection into “in-band” of the photovoltaic cell, l , and “out-of-band” of the photovoltaic cell as follows (17):

$$R = \frac{\epsilon_l(1-\rho_l)[1-\rho_b(1-\epsilon_b)]}{\epsilon_b(1-\rho_b)[1-\rho_l(1-\epsilon_l)]}, \quad (6)$$

where ϵ is the emissivity of the emitter surface and ρ is the reflectivity of an optical filter. Equation 6 enables one to analyze the effect of spectral control on conversion efficiency, the best value being 0, and the worst (i.e., no spectral control) being 1. Figure 4 demonstrates the maximum theoretical spectral efficiency from Chubb plotted against dimensionless bandgap energy for the full range of R -values. In the figure the Shockley and Queisser photovoltaic cell model assuming the open-circuit potential is equal to the bandgap potential was used by Chubb to understand the relationship between the peak spectral efficiency and the dimensionless bandgap. The probable range for the photovoltaic bandgaps ranging from 0.5 to 0.72 eV and operating temperatures from 800 to 1000 °C is highlighted in figure 4.

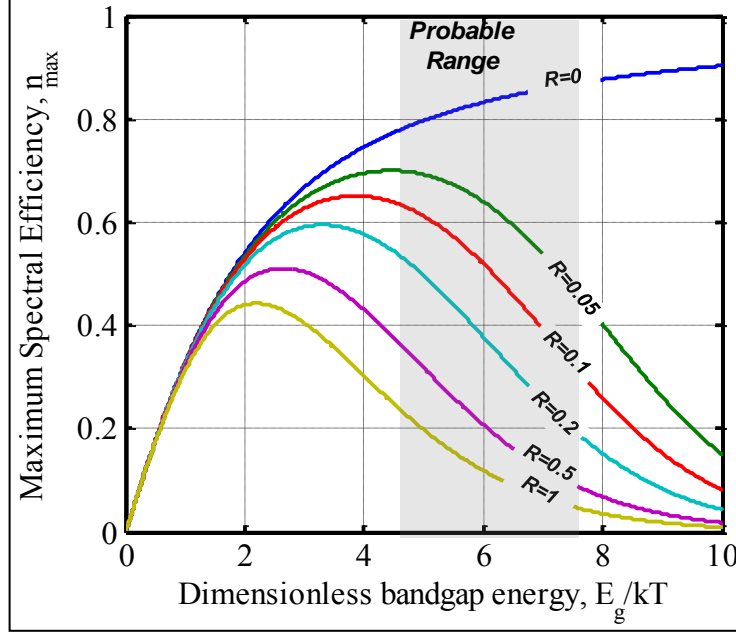


Figure 4. Maximum spectral efficiency from reference 17.

Figure 4 shows the influence that both the bandgap energy and the emitter temperature have on the conversion efficiency. Peak efficiency occurs when the photovoltaic cell bandgap and the temperature are “matched” with the emission temperature. R-values below 0.05 will be necessary to achieve peak efficiency potential in the range of bandgap energies and operating temperatures relevant for compact power applications. This demonstrates the need for approaches to minimize R. As noted before, the thermophotovoltaic efficiency without taking into account any efficiency owing to the burner is

$$\eta_{TPV} = \eta_{spectral}\eta_{cavity}\eta_{PV}. \quad (7)$$

The spectral efficiency can be computed by the in-band power delivered to the photovoltaic cell divided by the total in-band and out-of-band power emitted as follows:

$$\eta_{spectral} = \frac{\overline{Q_C}}{\overline{Q_E}} = \frac{A_C \int_0^{\lambda_g} q_{ic}(\lambda, T) d\lambda}{A_E \int_0^{\infty} q_{oE}(\lambda, T) d\lambda} = \frac{A_C \int_0^{\lambda_g} q_{ic}(\lambda, T) d\lambda}{A_E \left[\int_0^{\lambda_g} q_{oE}(\lambda, T) d\lambda + \int_{\lambda_g}^{\infty} q_{oE}(\lambda, T) d\lambda \right]}, \quad (8)$$

where A_C and A_E denote the collection area on the photovoltaic cell and the emitter area, respectively; q_{ic} denotes the thermal radiation reaching the photovoltaic cell; and q_{oE} denotes the radiation leaving the emitter. The term q_{ic} will be affected by the transmission and reflectance of elements between the emitter and the photovoltaic cell, such as an optical filter in addition to the reflectance properties of the photovoltaic cell.

A simplified thermophotovoltaic system having only a spectrally controlled emission and a photovoltaic cell can be analyzed to demonstrate the potential of a thermophotovoltaic converter.

For a system without a filter or reflector, i.e., spectral control comes solely from the emitter, the thermophotovoltaic efficiency without burner efficiency can be written as

$$\eta_{TPV} = \eta_{PV} F_{EC} \frac{\int_0^{\lambda_g} \varepsilon_E e_b(\lambda, T) d\lambda}{\int_0^{\infty} \varepsilon_E e_b(\lambda, T) d\lambda}. \quad (9)$$

The cavity efficiency is accounted for in equation 9 by the view factor, F_{EC} . In this analysis having only spectral control from the emitter, R from equation 6 is now the ratio of the out-of-band emissivity to the in-band emissivity $\varepsilon_{Eb}/\varepsilon_{El}$. From equation 9, the efficiency owing to the emitter is determined purely by the out-of-band emissivity. Power delivered to the photovoltaic cell, on the other hand, is greatly determined by the in-band emissivity and can be approximated by (17)

$$\frac{P}{A_C} \sim \frac{F_{CE}}{\lambda_g} \int_0^{\lambda_g} \varepsilon_E e_b(\lambda, T) d\lambda. \quad (10)$$

Figure 5 demonstrates the power per area for an example thermophotovoltaic conversion having an upper bound of a 0.6-eV bandgap photovoltaic cell with a maximum emitter emissivity of 1 and a lower bound of a 0.72-eV bandgap photovoltaic cell having an emissivity of 0.4. At a temperature of 1000 °C, the difference in power density can be five times for a photovoltaic cell efficiency of 30%. Figure 6 demonstrates the conversion efficiency calculated by equation 9 assuming $F_{EC} = 1$, $\eta_{pv} = 30\%$ for bandgaps of 0.72, 0.60, and 0.53 eV. The width of each curve represents R -values from 0.1 to 0.05. From figure 6, a 20% efficient thermophotovoltaic converter is feasible within the temperature range of 650 to 1200 °C if the advancements in selective emitters and photovoltaic cells highlighted in this report can be made.

Critical to note in equation 10 is that power depends heavily on both the in-band emissivity and energy bandgap of the photovoltaic cell. Thus, to maximize power output both bandgap and emissivity should also be maximized in addition to the operating temperature. When efficiency is concerned, however, it is most important that the emissivity of the out-of-band should be 0, while the in-band efficiency can be anything greater than 0 for maximum efficiency. This underscores the criticality to perform a tradeoff of power density and energy density when designing the thermophotovoltaic system.

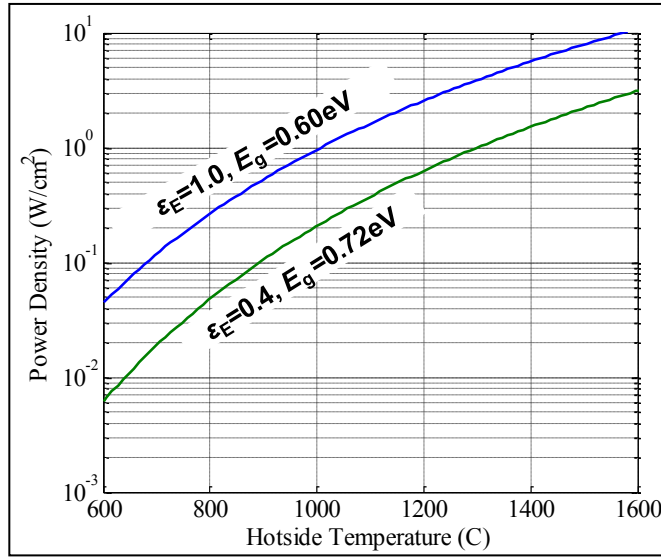


Figure 5. The power density of a notional thermophotovoltaic system is plotted vs. emitter temperature. A photovoltaic cell efficiency of 30% is used in the calculation of the power density.

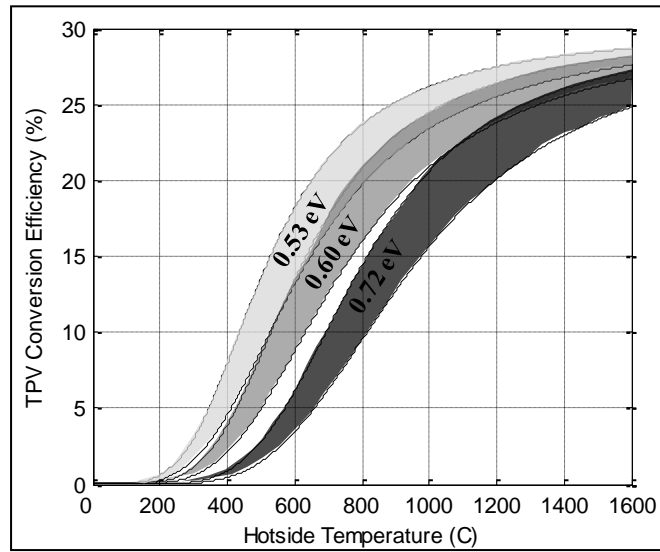


Figure 6. Thermophotovoltaic energy conversion efficiency for example bandgap energies assuming 30% photovoltaic conversion of in-band radiation and R-values ranging from 0.05 to 0.10 giving rise to the thickness of the curves.

Until recently, only naturally occurring spectral emitters such as platinum (Pt), rare-earth emitters (24) or gray-body emitters have been used. These either require high temperature for low R-values or have a high R-value such as Pt. Recently, emitters with engineered surfaces using photonic crystals or metamaterials have become promising for selective emission with good performance across a wide temperature range. These are patterns that can be used to create a photonic bandgap to control the light, i.e., a photonic crystal. A one-dimensional (1-D)

photonic crystal (e.g., Bragg gratings) is a stacking of layers alternating the index of refraction (18). A two-dimensional (2-D) photonic crystal consists of periodic structures fabricated on the surface of a material (18–21), and a three-dimensional (3-D) photonic crystal is a structure having a stacking of a 2-D lattice and is appropriately termed a “woodpile” (22).

Numerous groups have developed 1-D, 2-D, and 3-D structures on the surface of a solid emitter to demonstrate spectral control of the radiated emission (18–22). *Bermel et al.*, developed 1-D (silicon and silicon dioxide bi-layers) and 2-D (patterned tungsten) photonic crystals and evaluated the performance combined with a rugate filter, an emitter temperature of 1200 K, a view factor of 1, and a photovoltaic cell having a 0.547-eV bandgap (18). They calculated 45.6% of the emitted radiation to be in-band for the 1-D photonic crystal and 59.2% with the 2-D photonic crystal. A low emissivity material that can survive at high temperatures is highly desired. As such, the tungsten is an ideal candidate as used in the 2-D emitter from *Bermel et al.*, however coupling these structures to a heat source still remains a challenge due to significant thermal expansion mismatches (18). *Kirikae et al.*, etched 2-D structures directly on the surface of the silicon and coated the surface with Ti (20). They demonstrated improved conversion efficiency over blackbody (5.5%) of approximately 7.4% at 1200 °C using a germanium (Ge) low-bandgap photovoltaic cell. *Liu et al.*, described the use of metamaterials where a dielectric and metal are deposited directly on a silicon (Si) substrate (21). In their work they estimate very low emissivity in the out-of-band emission, suggesting that high R-values can be obtained. Although in their work they only demonstrated the technique to 300 °C it may be feasible at higher temperatures.

In addition to selective emitters, optical filters and reflectors can be integrated into the system to further improve the total efficiency. A high conversion efficiency was demonstrated by *Wernsman et al.*, who used a silicon nitride (Si_3N_4)/gold (Au) reflector on the backside of an InGaAs/InP (0.60 eV) diode with a dielectric stack on a highly n-doped InPaS plasma filter to achieve 23.6% conversion at 1039 °C (23). This suggests an R-value slightly above 0.1. Combined with selective emitters it may be feasible to decrease the R-value well below 0.1 to improve the efficiency. *Bermel et al.*, estimated the performance with an optimized rugate filter spaced closely to the 2-D tungsten photonic crystal to be 26.9% at 927 °C assuming a view factor of 1 and an InGaAsSb photovoltaic cell. Their estimation corresponds to an R-value below 0.05 suggesting that the combination of filters, reflectors, and selective emitters, once combined with an efficient heat source could yield very high efficiencies.

2.5 Thermophotovoltaic and Thermoelectric Conversion Efficiency Comparison

Many technologies have been investigated for TEC. Of them, thermoelectric and thermionic energy conversion for a continuous temperature difference has been evaluated most with thermoelectric having some commercial availability. In fact, NASA and other space agencies around the world have used both thermoelectric and thermionic generators for their deep space missions using a radioisotope heat source.

Thermoelectric has been developed for NASA power generation in remote areas of space as well as for cooling application. Thus, >5% for radioisotope thermoelectric generator (RTG) using very reliable material systems can be achieved. Thermoelectric materials are continually being improved with a focus on increasing electrical conductivity, reducing thermal conductivity and improving the Seebeck coefficient.

TEC efficiency can be calculated using the Carnot efficiency and the figure of merit for thermoelectric materials, zT as follows

$$\eta_{TE} = \frac{(T_{Hot}-T_{Cold})}{T_{Hot}} \times \frac{\sqrt{1+zT}-1}{\sqrt{1+zT}+T_{Cold}/T_{Hot}}, \quad (11)$$

where T_{Hot} and T_{Cold} are the temperatures of the hot side of the thermoelectric and cold side of the thermoelectric module respectively (25). The figure of merit zT is:

$$zT = \alpha^2 / (\kappa\rho), \quad (12)$$

where α is the Seebeck coefficient, κ is the thermal conductivity, ρ is the electrical resistivity, and T is the average temperature from the hot-side to the cold-side ($(T_{Hot} + T_{Cold})/2$) of the thermoelectric junction. Commercial devices are available for up to 230 °C (200 °C for maximum reliability) on the hot side with approximately 5% conversion efficiency, equating to a ZT of approximately 0.5 (26). Higher temperature and higher zT materials have been demonstrated within the research and development (R&D) community, for example, skutterudite materials have the potential to produce 14.7% efficiency at 700 °C with a 27 °C cold side temperature, equating to approximately a $ZT = 0.75$ (27). Figure 7 plots the theoretical TEC efficiency for equation 7 for ZT of 0.5, 1.0, and 2.0. The latter is an upper end of the most recent advances in high temperature thermoelectric materials and multi-junction devices. Most demonstrated thermoelectric modules (single or multi-stacks) fall below $ZT = 1$.

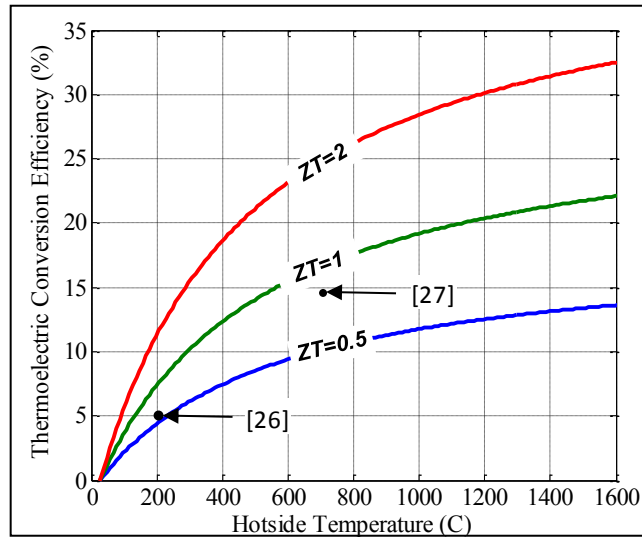


Figure 7. Thermoelectric conversion efficiency is plotted vs. the temperature of the hot side with a cold side temperature at 27 °C.

Figure 8 shows a comparison of thermoelectric and thermophotovoltaic thermal conversion efficiency versus the hotside temperature. The cold side temperature of the thermoelectric and photovoltaic cell are assumed to be 27 °C and photovoltaic cell efficiency of 30% for three energy bandgaps of 0.53, 0.60, and 0.72 eV. Note that the view factor for the thermophotovoltaic is assumed to be 1 (see figure 9). Convective and conduction losses between the hot-side and cold-side are also neglected for both, which is appropriate for vacuum packaged converters. Regardless, figure 8 demonstrates both thermoelectric and thermophotovoltaic may be able to provide conversion efficiencies greater than 10% at temperatures generally exceeding 500 °C. For most applications this may be sufficient to create a high energy dense power source. At lower temperatures, where energy scavenging applications exist, thermoelectric conversion has a distinct advantage over thermophotovoltaic conversion.

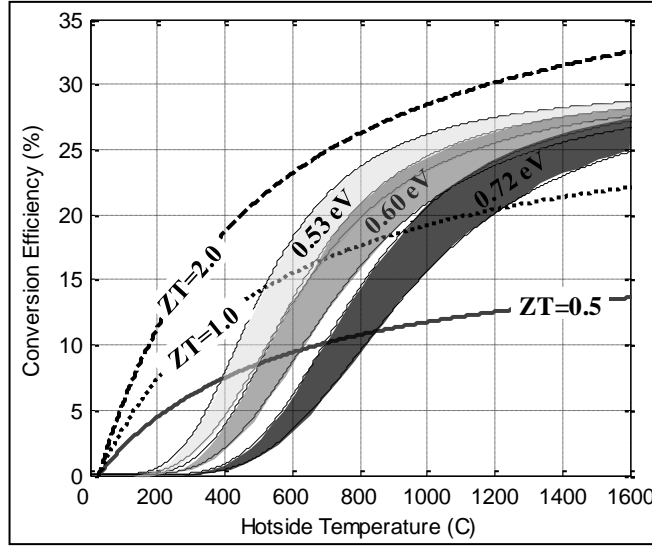


Figure 8. Thermophotovoltaic and thermoelectric conversion efficiency plotted vs. temperature.

The view factor becomes an important consideration in small systems where the surface area to gap ratio can be small. This parameter describes the amount of radiation lost or leaked out the edge of the cavity and depends on the geometry of the emitter and photovoltaic cell surfaces as well as the spacing between them. The view factor is plotted in figure 9 using the equation for identical, parallel, directly opposed squares in Chubb (17). When the ratio becomes very large, i.e. above a ratio of 100, then greater than 98% of the radiation emitted by the emitter surface is received at the photovoltaic cell surface. At low ratios, for example, a 1 cm x 1 cm surfaces spaced at 0.1-cm distance (ratio of 10), the view factor is reduced to below 83%. It is therefore essential to minimize the spacing between the emitter and the photovoltaic cell such that a high number of photons reach the photovoltaic cell surface.

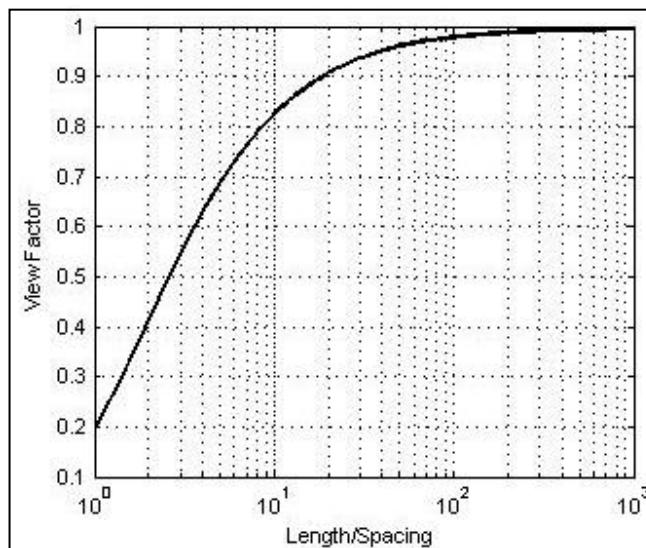


Figure 9. Plot showing the view factor of equal squares vs. the ratio of the square length to the spacing.

2.6 Thermophotovoltaic Technology Discussion

In addition to improvements in tailoring the radiated spectrum and in the photovoltaic cell, there are other areas of the thermophotovoltaic system that need to be addressed to achieve optimum conversion efficiencies. Most notable are the techniques to package together the heat source, emitter, and photovoltaic cell including a sustained inert cavity between the emitter and the photovoltaic cell with high thermal efficiency as well as reject the unused heat from the photovoltaic cell to maintain peak cell efficiency.

2.6.1 Thermophotovoltaic Packaging and Practical Considerations

High temperature and hermetic packaging techniques are important to maximize the total thermophotovoltaic system efficiency. Providing an inert atmosphere with low thermal conductivity within the optical cavity will be critical for both emitter lifetime and low thermal loss. Mesoscale systems, having cavity spacing well beyond 1 mm such as the 25-W demonstration thermophotovoltaic power source by Doyle et al. (28) used a hermetically sealed system to provide an inert atmosphere around the high temperature components and a low thermal conductivity.

Vacuum packaging to the mTorr range to achieve thermal conductivity below mW/mK is greatly beneficial for small-scale thermophotovoltaic systems where the spacing between the emitter and the photovoltaic cell is in the millimeter range and below. Numerous vacuum packaging techniques exist for microelectronic and microelectromechanical system (MEMS) technologies (29, 30). These works are mainly focused on reduction of dampening effects for high-Q factors in applications such as gyroscopes or accelerometers; however, they could be applied to microscale combustion devices and thermophotovoltaic sources at extremely small scale.

2.6.2 Heat Exchanger

The photovoltaic cell will be heated by the unconverted radiated energy. The performance of the photovoltaic cell decreases with temperature and thus the unconverted energy, which results in heat generation, must be carried away by a heat exchanger. For example, Wernsman et al., showed a spectral performance decrease from 22.3% to 18.7% when the photovoltaic cell temperature was increased from 24 to 64 °C (23). If a thermophotovoltaic system has a conversion efficiency of 10% and can generate 0.5 W/cm² like demonstrated by Wernsman et al., then 4.5 W/cm² of heat, assuming a view factor of 1, must be removed by the heat exchanger to maintain the photovoltaic cell at room temperature. This level of cooling will most likely require forced convection cooling or a novel design for integrating a large surface area heat exchanger into the package. Heat exchangers may use the fuel as the coolant or include a fan to provide forced air convective cooling. Both approaches require the mass and volume of the heat exchanger and electrical power to operate the fan.

2.6.3 Future High Power Density Thermophotovoltaic Strategies

Up to now, only far-field configurations have been discussed since it is the most relevant for near-term applications. However, a rising field of study in nanoscale thermal radiation is advancing and could greatly alter the way thermophotovoltaic performs. When the gap between the emitter and collector (photovoltaic cell) is close to the wavelength or below, heat transfer is dominated by evanescent wave coupling and photon tunneling (32). Basu et al., provide a theoretical system design using a tungsten emitter held at an extreme temperature of 1727 °C and an InGaSb photovoltaic cell. They evaluated the gap spacing between the emitter and the photovoltaic cell and estimated the power and conversion efficiency. Their estimations were based on the penetration depth of the thermal radiation into the cell using the fluctuation-dissipation theorem and the dyadic Green's function of Maxwell's equations for a multilayered structure. In their analysis they find a peak theoretical efficiency similar to far-field thermophotovoltaic, however, with an increasing power transfer as the gap goes below 200 nm. At 10 nm, their analysis suggests 100 W/cm²; a factor of 10 more than is available with cavity gaps above the peak emission wavelength.

In addition to thermophotovoltaic conversion, near-field thermal transport has applications in nano-fabrication (33–35) and near-field imaging (36). The theoretical foundation for near-field heat transfer has been well developed over the past few years, but limited experimental work has been done to verify concepts with material systems relevant to thermophotovoltaic applications.

3. TEC System

It is important to recognize that most literature values for efficiency only speak about the η_{TEC} conversion efficiency. One must understand the losses associated with all components of the conversion system to compare to, for example, a battery that has minimal parasitic loss. The dominant sources of energy loss within the conversion system include thermal losses associated with the burner thermal efficiency, chemical conversion efficiency (i.e., fuel + air produce carbon dioxide [CO₂] and water [H₂O] for 100% efficiency), thermal-to-electric conversion efficiency, and the balance-of-plant (BoP).

Energy conversion is accomplished in a system that is comprised of the TEC and all of the components required providing heat generation, fluid pumping, control, sensing, and power management. For compact TEC as well as fuel cell systems, the BoP will often comprise most of the weight of the conversion system. This weight affects the overall power and energy density as well as the scalability. At high powers or long durations, the fuel and conversion efficiency dominate; however, at low power (generally <10 W) or short durations, the BoP and system dominates. Great improvements can be had in developing low-power, lightweight BoP for compact power applications.

In addition to the energy conversion system, the fuel of choice influences the performance of the system. Table 1 provides information on the fuels of interest for portable power applications. Methanol and hydrogen are also included in the table to compare with fuel cell technology. A few items are important to point out. First, the phase that the fuel is in at room temperature and ambient pressures determines the storage efficiency as well as the need for atomization. Liquids can be stored in lightweight containers, taking up approximately 10% of the weight of the fuel. On the other hand, liquid fuels also require atomization or vaporization. Efficient and robust means to accomplish this are still being developed. Gaseous fuels like butane and propane may have higher energy content and not require means to evaporate, but require storage under high pressure, and therefore, heavy storage containers. The storage thus consists of 40% of the combined fuel and fuel tank weight.

When comparing the possible fuels for compact TEC power generation (table 1), it is useful to make a comparison with the fuels used in fuel cell technologies. Although current fuel cells offer high chemical-to-electrical conversion efficiency the energy density is often hampered by the use of a fuel having low energy content when compared to hydrocarbons or fuels having low storage efficiencies. Methanol fuel cells are the state of the art for compact power and have lower energy content than other fuels. Hydrogen has extreme energy; however the storage media is still a large area of research and as previously discussed has low storage efficiency.

Table 1. Characteristics of candidate fuels (37).

	Energy Content (kW·h/kg)	Boiling Point (°C)	Density (kg/m ³)	Storage Medium	Storage Efficiency (% wt.)
JP8	11.9	290	837	Low-pressure tank	90%
Butanol (biomass)	9.5	118	810	Low-pressure tank	90%
Propane	12.9	-42.1	507	High-pressure tank	60%
Butane	12.6	-0.5	585	High-pressure tank	60%
Hydrogen	33.4	-252.87	0.67 (gas)	NaBH ₄ (38)	9%
Methanol	5.6	65	794	Low-pressure tank	90%

3.1 Heat Source

The heat source is a critical determinant of the application space and efficiency of the TEC system. Heat useful for power generation from a TEC system can come from numerous sources including solar (39), combustion, or radioisotope (27) and highly depends on the intended application of the power source.

For high energy dense and compact power sources requiring durations of days or weeks, combustion is the most suitable source of heat. When compared to fuel cells, TEC using a combustion-based heat source will have the added benefit of fuel flexibility. For portable power applications meso- and micro-scale combustion are the most promising. Numerous works have provided information for large-scale and microscale combustion, however not focused on portable power production. The area of microscale combustion has typically focused on chemical processing and does not necessarily optimize to deliver heat to a specific surface; as such heat recuperation is often ignored. Numerous compact combustors have been developed of which notable ones are from references 40–45.

The thermal efficiency of the combustion heat source is determined by the heat loss to the surrounding environment through convection, conduction, and radiation from each surface as well as the heat being carried away by the exhaust. Choice of materials and packaging techniques can minimize convection, conduction, and radiation; however, heat lost through the exhaust requires integrated heat transfer structures to recuperate the heat into the incoming fluid streams. More than 50% of the thermal power of the combustor can be lost to the exhaust as it is often a very low resistive path. In addition to improving thermal efficiency, hotter temperatures can be maintained within the combustion zone and TEC hotside. Hotter temperatures within the combustion zone broaden flammability limits for more robust combustion as well as reduce combustion timescales for higher combustion efficiency and more compactness. Hotter temperatures at the TEC hotside will enable a higher TEC efficiency as demonstrated by figure 8. Thermal and chemical conversion efficiencies, η_{heat} , can be greater than 60% using heat recuperated from the exhaust to pre-heat the incoming fuel and air mixture as demonstrated by Bijjula et al. (40).

Compact combustion has applications beyond power generation and thus has had extensive research devoted to it. Recent review papers outline the challenges and research areas for both homogeneous and heterogeneous combustion within the scales of interest for compact power (46, 8). Although power generation is a prime application as all reviews indicate, other applications exist such as sensors, chemical processors, and lab-on-a-chip. The largest area of research is in the modeling of the combustion process for the complex fuels and identifying the operating space, such as flammability limits, for the compact combustors. As the geometry scales, the reaction pathways and mechanisms will change due to a shift of the dominant mass transfer mechanism. This results in a change in the reaction rates and flammability limits. Some numerical predictions and experimental results of flammability limits can be found; however, most focus on gaseous fuels. More research is necessary to include liquid fuels within the combustion platforms such that a truly multi-fuel heat source can be integrated within the TEC system.

3.2 Balance-of-plant Components

The overall TEC system energy and power density depend on the parasitic loss and weight (not taken into account in equation 1) of the BoP and increases in dependence as the system scales down. High average power and a long duration require fuel amounts that dominate the weight of the power source, thus the energy and power density of the system becomes that of the fuel. The amount of fuel may be small at low average power requirements and short durations, thus the total weight will be dominated by the TEC system.

Much of the TEC system weight is due to the BoP or ancillary components such as a liquid pump, air pump, heat sink, air fan and packaging materials like plumbing, connections and insulation. The pumps and fans are active BoP components and are required to maintain optimal performance (e.g., to maintain a constant temperature). Miniature pumps for fuel and air handling can be evaluated to indicate the power draw and weight affects on the overall system. Miniature liquid pumps, often times piezoelectric-based diaphragm pumps, have a range of electrical power requirements of <200 mW and weights of 2–3 g (e.g., mp6 micropump from Bartels mikrotechnik [47]). Miniature air pumps have a range of electrical power requirements of 500 to 700 mW and a range of weights of 15 g (<1 L/min) to 50 g for approximately 1 L/min flows (e.g., EC Series 100 from Schwarzer Precision [48]). The heat sink required to maintain the cold side of the TEC will have a similar weight as the air pump or more (49). If the converter is a solid piece of silicon which has a density of 2330 kg/m³ then a 27 cm³ volume would weigh 63 g. The core BoP can weigh more than 2 or 3 times that weight; therefore, the BoP dictates the total weight of the conversion system without the fuel or fuel tank.

State-of-the art fluidic components use Microsystems technology to develop the individual components and can still improve the pumping efficiency, especially at a low flow rate. The mechanical power required to pump air at 1 L/min through a system having a pressure drop of 689 Pa (0.1 psi) is approximately 10 mW. Compared to the state-of-the art fluidic pumps such as

the ones described above the electrical-to-mechanical conversion efficiency is only a few percent at best. This parasitic loss should be significantly reduced for low-power sources in the Watt-level range. Few groups have focused on developing passive or self operating/limiting systems to eliminate the need for power-hungry BoP. Some examples of these can be found in micro fuel cell research that uses Microsystems approaches to achieve self-regulating or self-pumping of the fuel or passive air delivery (50–52).

Electronics are another component of the BoP and are required to convert the extracted power and control, for example, the operation of the photovoltaic cell. These electronics can be very light; however, the conversion efficiency should be taken into consideration as there is a parasitic loss associated with them. For example, Pilawa-Podgurski et al., developed a low-power maximum power point tracker for thermophotovoltaic generators and demonstrated a converter efficiency of 90% (53).

3.3 TEC System Power Density and Conversion

A number of parameters must be considered when evaluating the power and energy density of a power generation mechanism. The total weight can be broken up into the system weight, the weight of the fuel, and the weight of the fuel storage. In addition to the weight, the parasitic power loss, or electrical power requirements for the active BoP components are used to determine the power and energy density. The duration of the power draw and the average power requirement are determined by the application space. On one hand, UAV applications may require a large average power, for example, 100-W electrical, for a minimum duration of a few hours. On the other hand, expeditionary power for personal power sources may require on the order of 10-W electrical, a lower power, however require it for multiple days. In some cases, the system weight is determined by the average power draw. The duration requirement will determine the amount of fuel required given the conversion efficiency, and therefore, the weight of the fuel and the weight of the fuel storage.

Many works focused on Microsystems technology assume the weight of the system will be negligible. This may be the case for the converter, such as a micro gas turbine generator (6) or micro-thermophotovoltaic (18, 20); however, the BoP is often neglected. Although the goal for Microsystems designers is to create a wholly integrated system such that the system weight is negligible, this will only be the case for long mission durations when a large amount of fuel is required. There is still a technology gap to integrate all BoP in a compact power form; however, Microsystems technology offers a promising path.

Figure 10 demonstrates different durations and average powers which span the space of sensor electronics (low power, long duration) to UAV (high power, long duration) applications. Figure 10 was derived using JP8 with an energy density of 11.9 W·h/kg and 90% storage efficiency scaled linearly with duration and a 10% overall TEC conversion. The TEC and BoP (not fuel or tank) is varied between 0.1 and 0.5 kg considered to be an overestimate at low average powers and aggressive at high average powers. For short durations, when the system weight dominates

for low power, the power density and energy density varies more than two orders of magnitude between the different average powers. At long durations the fuel dominates the system weight, 72 h, for example, they vary less than an order of magnitude for each.

The necessary TEC conversion efficiency can be determined in order to compete with battery technology. This allows one to understand the application space for TECs. A comparison of the potential TEC power and energy density to battery technology is provided in figures 11 and 12 for 24- and 72-h durations against the conversion efficiency. Even low conversion efficiency, <5% competes with state-of-the-art Li-ion rechargeable batteries. Comparison to Li-air, a higher energy dense and power dense technology requires a TEC to be greater than 10% for 72-h duration and approximately 15% for 24-h duration.

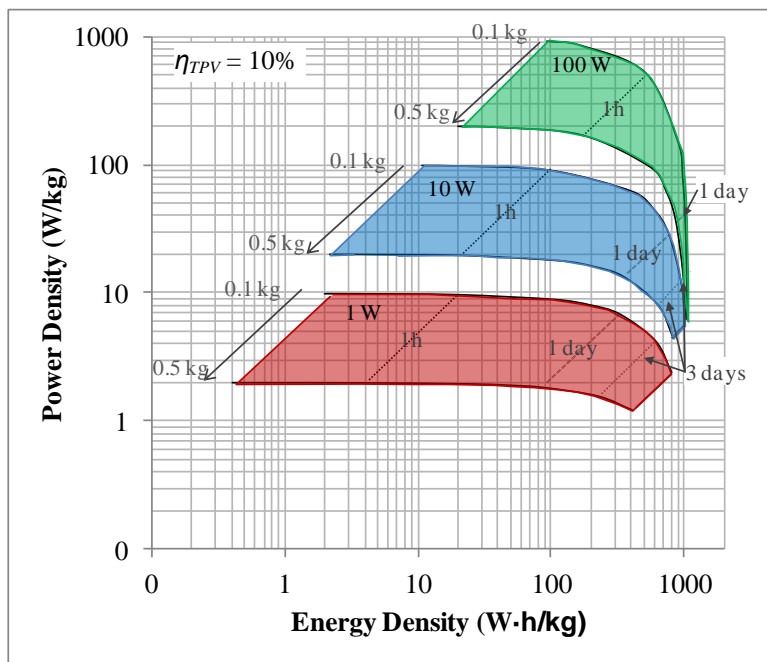


Figure 10. Ragone plot for TEC assuming 10% conversion efficiency and assuming fuel storage is 10% of fuel weight for JP-8 fuel.

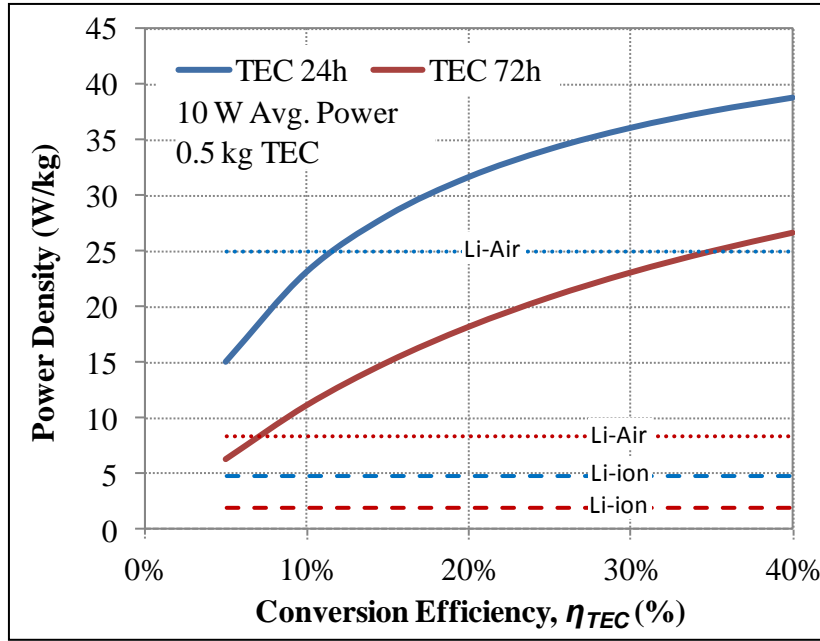


Figure 11. Power density plotted vs. TEC conversion efficiency for durations of 24 and 72 h. Li-ion (dashed line) and Li-Air (dotted line) battery technologies are plotted for comparison.

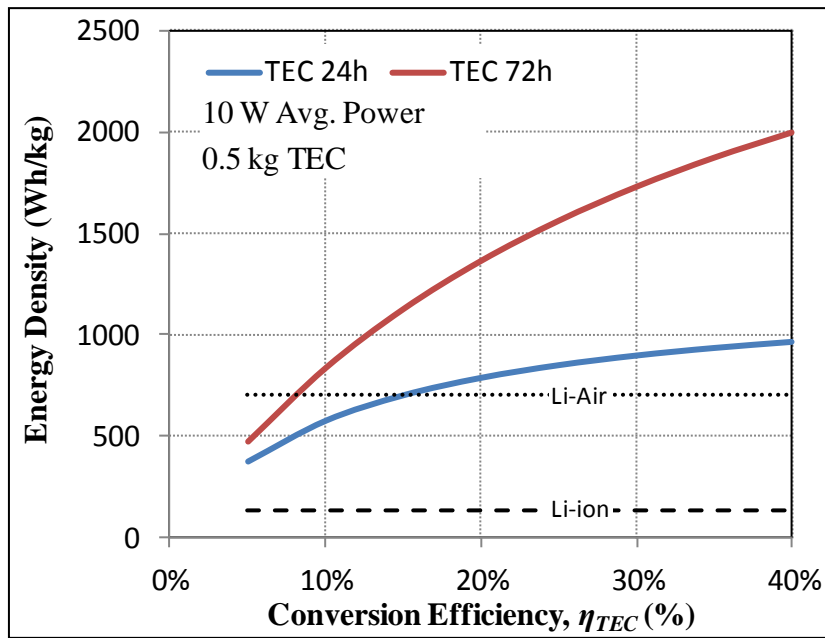


Figure 12. Energy plotted vs. TEC conversion efficiency for duration of 24 and 72 h. Li-ion (dashed line) and Li-Air (dotted line) battery technologies are plotted for comparison.

Although conversion efficiency is a key performance metric, other characteristics of the power source should be kept in mind. The ability to instantly recharge by filling the tank with more fuel

or swapping fuel cartridges can be a great benefit of fuel cells and TEC when compared to batteries. Additionally, this power density and energy density presented in this report is for a system with a full fuel tank. As fuel is used, the overall weight is reduced something that cannot occur with a battery. As previously stated, the resupply could also be eased by allowing a multi-fuel burner capability.

From figure 6, R values greater than 0.1 are required to achieve spectral efficiencies/ photovoltaic cell greater than ~15% at temperatures close to 1000 °C. From the previous capabilities description, it may be feasible to develop a TEC system in the near future having $\eta_{HEAT} = 80\%$ burners and a cavity efficiency of 80%. From this a total thermophotovoltaic system efficiency of 10% could be possible.

To achieve an overall conversion efficiency, $\eta_{TEC} = 15\%$ all facets of TEC and thermophotovoltaic need to be optimized with research continuing in meso/microscale combustion for an efficient heat source. High temperature vacuum packaging and thermal design, novel selective emitter materials, and high efficiency, low bandgap photovoltaic cells are key items to be addressed. It is feasible that if peak R-values can be applied less than 0.05, photovoltaic cells having a bandgap of 0.53 eV or below and a conversion efficiency reaching 30%, 90% heat delivery, and view factors of >90%, then a total conversion efficiencies greater than 20% may be possible.

4. Conclusions

Advancements in photovoltaic, thermal emission and compact liquid fueled combustion sources enable thermophotovoltaic energy conversion to compete with battery and fuel cell technology for compact power applications. This report highlighted all components of the TEC system including the balance-of-plant and provided a review of the state of the art. Evaluation of each component performance led to a determination that a 10% efficient thermophotovoltaic power source could be realized by integrating state-of-the art components. Such efficiency could lead to a power source that approaches an energy density of 1000 W·h/kg when long durations are needed all while using a combustion-based, fuel flexible heat source.

Continued research on each of the thermophotovoltaic components can greatly enhance the capability extending the use to short durations or increasing the energy density. Specific research areas include reduction of the photovoltaic cell bandgap and Auger recombination, improved emitters using photonic crystals to tailor the emission spectrum, and developing efficient heat recuperation within a combustion-based heat source. It is feasible these improvements can lead to TEC efficiencies greater than 20% with temperatures below 1000 °C.

5. References

1. Ultralife. Li-145 Ultralife battery datasheet, UBBLO6, 2010 battery.
2. Lawrence Livermore National Laboratory. www.lanl.gov/orgs/tt/pdf/techs/dmfc_entry.pdf (accessed February 2012).
3. Awilco Multiplex. http://www.awilco-multiplex.dk/files//pdf/Fuel%20cells/Military/SFC_FC_250_datasheet.pdf (accessed February 2012).
4. EFOY Web site. <http://www.efoy-comfort.com/technical-data> (accessed February 2012).
5. Marlow Industries. TG 12-2.5-01L datasheet, DOC # 102-0341 REV F.
6. Peck, J.; Jacobson, S. A.; Waitz, I. A. Design and Characterization of a Liquid-Fueled Microcombustor. *Journal of Engineering for Gas Turbines and Power-Transactions of the Asme* **Jul 2011**, 133.
7. Fu, K.; Knobloch, A. J.; Martinez, F. C.; Walther, D. C.; Fernandez-Pello, C.; Pisano, A. P.; Liepmann, D. Design and Fabrication of a Silicon-based MEMS Rotary Engine. *Micro-Electro-Mechanical Systems (MEMS). 2001 ASME International Mechanical Engineering Congress and Exposition*, 01 2001.
8. Walther, D. C.; Ahn, J. Advances and Challenges in the Development of Power-generation Systems at Small Scales. *Progress in Energy and Combustion Science* **Sep 2011**, 37, 583–610.
9. Wedlock, B. D. Thermo-Photo-Voltaic Energy Conversion. *Proceedings of the IEEE* **1963**, 51, 694-&, 1963.
10. Hernquist, K. G.; Kanefsky, M.; Norman, F. H. Thermionic Energy Converter. *RCA Rev.* **1959**, 19.
11. El-Genk, M. S. Deployment History and Design Considerations for Space Reactor Power Systems. *Acta Astronautica* **May–Jun 2009**, 64, 833–849.
12. Nelson, R. E. A Brief History of Thermophotovoltaic Development. *in Semiconductor Science and Technology* **2003**, 18, 141–143.
13. Guazzoni, G.; Matthews, S. A Retrospective of Four Decades of Military Interest in Thermophotovoltaics. *in AIP Conference Proceedings* **2004**, 738, 3.

14. Dashiell, M.; Beausang, J.; Ehsani, H.; Nichols, G.; Depoy, D.; Danielson, L.; Talamo, P.; Rahner, K.; Brown, E.; Burger, S.; Fourspring, P.; Topper, W.; Baldasaro, P.; Wang, C.; Huang, R.; Conners, M.; Turner, G.; Shellenbarger, Z.; Taylor, G.; Li, J.; Martinelli, R.; Donetski, D.; Anikeev, S.; Belenky, G.; Luryi, S. Quaternary InGaAsSb Thermophotovoltaic Diodes. *IEEE Transactions on Electron Devices* **Dec 2006**, *53*, 2879–2891.
15. Rohr, C.; Abbott, P.; Ballard, I.; Connolly, J.; Barnham, K.; Mazzer, M.; Button, C.; Nasi, L.; Hill, G.; Roberts, J.; Clarke, G.; Ginige, R. InP-based Lattice-matched InGaAsP and Strain-compensated InGaAs/InGaAs Quantum Well Cells for Thermophotovoltaic Applications. *Journal of Applied Physics* **1 Dec 2006**, *100*, 114510-1–114510-6.
16. Tuley, R. S.; Nicholas, R. J. Band Gap Dependent Thermophotovoltaic Device Performance using the InGaAs and InGaAsP Material System,. *Journal of Applied Physics* **15 Oct 2010**, *108*.
17. Chubb, D. L. *Fundamentals of Thermophotovoltaic Energy Conversion*. Amsterdam: Elsevier, 2007.
18. Bermel, P.; Ghebrehrehan, M.; Chan, W.; Yeng, Y.; Araghchini, M.; Hamam, R.; Marton, C.; Jensen, K.; Soljacic, M.; Joannopoulos, J.; Johnson, S.; Celanovic, I. Design and Global Optimization of High-efficiency Thermophotovoltaic Systems. *Optics Express* **13 Sep 2010**, *18*, A314–A334.
19. Chen, Y.; Tan, K. The Profile Optimization of Periodic Nano-structures for Wavelength-selective Thermophotovoltaic Emitters. *International Journal of Heat and Mass Transfer* **Nov 2010**, *53*, 5542–5551.
20. Kirikae, D.; Suzuki, Y.; Kasagi, N. A Silicon Microcavity Selective Emitter with Smooth Surfaces for Thermophotovoltaic Power Generation. *Journal of Micromechanics and Microengineering* **Oct 2010**, *20*, 7.
21. Liu, X.; Tyler, T.; Starr, T.; Starr, A.; Jokerst, N.; Padilla, W. Taming the Blackbody with Infrared Metamaterials as Selective Thermal Emitters. *Physical Review Letters* **18 Jul 2011**, *107*, 045901-1–045901-4.
22. Nagpal, P.; Han, S.; Stein, A.; Norris, D. Efficient Low-Temperature Thermophotovoltaic Emitters from Metallic Photonic Crystals. *Nano Letters* **10 Oct 2008**, *8*, 3238–3243.
23. Wernsman, B.; Siergie, R. R.; Link, S. D.; Mahorter, R. G.; Palmisiano, M. N.; Wehrer, R. J.; Schultz, R. W.; Schmuck, G. P.; Messham, R. L.; Murray, S.; Murray, C. S.; Newman, F.; Taylor, D.; DePoy, D. M.; Rahmlow, T. Greater Than 20% Radiant Heat Conversion Efficiency of a Thermophotovoltaic Radiator/Module System using Reflective Spectral Control. *IEEE Transactions on Electron Devices* **Mar 2004**, *51*, 512–515.

24. Ferguson, L.; Fraas, L. Matched Infrared Emitters for use with GaSb TPV Cells. *AIP Conference Proceedings*, 01 1997.
25. Snyder, G. J.; Ursell, T. S. Thermoelectric Efficiency and Compatibility. *Physical Review Letters* **3 Oct 2003**, 91.
26. TG 12-2.5-01L datasheet from Marlow Industries, DOC # 102-0341 REV F.
27. El-Genk, M. S.; Saber, H. H.; Caillat, T. Efficient Segmented Thermoelectric Unicouples for Space Power Applications. *Energy Conversion and Management* **Jul 2003**, 44, 1755–1772.
28. Doyle, E.; Shulka, K.; Metcalfe, C. Development and Demonstration of a 25 Watt Thermophotovoltaic Power Source for a Hybrid Power System. 2001.
29. Najafi, K. Micropackaging Technologies for Integrated Microsystems: Applications to MEMS and MOEMS. *Proceedings of the SPIE - The International Society for Optical Engineering* **2003**, 4984 (01).
30. Ramesham, R.; Kullberb, R. C. Review of Vacuum Packaging and Maintenance of MEMS and the use of Getters Therein. *Journal of Micro-Nanolithography MemS and Moems* **Jul–Sep 2009**, 8.
31. Min, M.; Zing, Z.; Yunsong, Q.; Yangfei, Z.; Yufeng, J.; Hua, G. A LTCC Microsystem Vacuum Package Substrate with Embedded Cooling Microchannel and Pirani Gauge. *Proceedings of the 2010 5th IEEE International Conference on Nano/Micro Engineered and Molecular Systems (NEMS 2010)*, 01 2010.
32. Basu, S.; Zhang, Z.; Fu, C. Review of Near-field Thermal Radiation and its Application to Energy Conversion. *International Journal of Energy Research* **25 Oct 2009**, 33, 1203–1232.
33. Lin, Z. W.; Wei, Q. H.; Zhang, X. Surface Plasmon Interference Nanolithography. *Nano Letters* **May 2005**, 5, 957–961.
34. Wang, L., Uppuluri, S. M.; Jin, E. X.; Xu, X. F. Nanolithography using High Transmission Nanoscale Bowtie Apertures. *Nano Letters* **Mar 2006**, 6, 361–364.
35. Lee, B. J.; Chen, Y. B.; Zhang, Z. M. Confinement of Infrared Radiation to Nanometer Scales Through Metallic Slit Arrays. *Journal of Quantitative Spectroscopy & Radiative Transfer* **Mar 2008**, 109, 608–619.
36. Wilde, Y.; Formanek, F.; Carminati, R.; Gralak, B.; Lemoine, P.-A.; Joulain, K.; Mulet, J.-P.; Chen, Y.; Greffet, J.-J. Thermal Radiation Scanning Tunnelling Microscopy. *Nature* **7 Dec 2006**, 444, 740–743.
37. GREET Transportation Fuel Cycle Analysis Model, GREET 1.8b, developed by Argonne National Laboratory, Argonne, IL, released May 8, 2008.

38. Delmas, J.; Laversenne, L.; Rougeaux, I.; Capron, P.; Garron, A.; Bennici, S.; Swierczynski, D.; Auroux, A. Improved Hydrogen Storage Capacity Through Hydrolysis of Solid NaBH(4) Catalyzed with Cobalt boride. *International Journal of Hydrogen Energy* **Feb 2011**, *36*, 2145–2153.
39. Imenes, A. G.; Mills, D. R. Spectral Beam Splitting Technology for Increased Conversion Efficiency in Solar Concentrating Systems: a Review. *Solar Energy Materials and Solar Cells* **Oct 2004**, *84*, 19–69.
40. Bijjula, K.; Wetzel, E. D.; Vlachos, D. G. Optimization of Integrated Thermoelectric/Microcombustor Devices. presented at the *PowerMEMS 2009*, Washington, DC, 2009.
41. Federici, J. A.; Norton, D. G.; Bruggemann, T.; Voit, K. W.; Wetzel, E. D.; Vlachos, D. G. Catalytic Microcombustors with Integrated Thermoelectric Elements for Portable Power Production. *Journal of Power Sources* **27 Oct 2006**, *161*, 1469–1478.
42. Kamijo, T.; Suzuki, Y.; Kasagi, N. Micro Catalytic Combustor with Pd/Nano-porous Alumina for High-temperature Application. *7th JSME-KSME Thermal and Fluids Engineering Conference. TFEC 2008*, 01 2008.
43. Arana, L. R.; Schaevitz, S. B.; Franz, A. J.; Schmidt, M. A.; Jensen, K. F. A Microfabricated Suspended-tube Chemical Reactor for Thermally Efficient Fuel Processing. *Journal of Microelectromechanical Systems* **Oct 2003**, *12*, 600–612.
44. Kuo, C. H.; Ronney, P. D. Numerical Modeling of Non-adiabatic Heat-recirculating Combustors. *Proceedings of the Combustion Institute* **2007**, *31*, 3277–3284.
45. Deng, W.; Klemic, J. F.; Li, X.; Reed, M. A.; Gomez, A. Liquid Fuel Microcombustor using Microfabricated Multiplexed Electrospray Sources. *Proceedings of the Combustion Institute* **2007**, *31*, 2239–2246.
46. Ju, Y.; Maruta, K. Microscale Combustion: Technology development and fundamental research. *Progress in Energy and Combustion Science* **2011**, *37*, 669–715.
47. Bartels Mikrotechnik GmbH Web site, 2010. <http://www.micro-components.com/index.php/micropump-information/technical-data-mp6>. (accessed February 2012).
48. Schwarzer Precision Web site. 2010 datasheet for the EC Series 100. <http://www.schwarzer.com>. (accessed February 2012).
49. Heymann, D. B.; Meyer, C. D.; Jankowski, N. R.; Morgan, B. C. Modeling the System Impact of Cooling Performance on a Compact Thermoelectric Generator. in *PowerMEMS 2009*, Washington, DC, 2009, pp. 601–604.

50. Moghaddam, S.; Eakkachai, P.; Masel, R. I.; Shannon, M. An Enhanced Microfluidic Control System for Improving Power Density of a Hydride-based Micro Fuel Cell. *Journal of Power Sources* **2 April 2010**, 195, 1866–1871.
51. Meng, D. D.; Kim, C.-J. Micropumping of Liquid by Directional Growth and Selective Venting of Gas Bubbles. *Lab on a Chip* **2008**, 8, 958–968.
52. Yingli, Z.; Junsheng, L.; Chong, L.; Tianliang, M.; Liding, W. Development of a Passive Direct Methanol Fuel Cell (DMFC) Twin-stack for Long-term Operation. *Journal of Power Sources* **5 Sept 2009**, 193.
53. Pilawa-Podgurski, R.C.N.; Pallo, N. A.; Chan, W. R.; Perreault, D. J.; Celanovic, I. L. Low-power Maximum Power Point Tracker with Digital Control for Thermophotovoltaic Generators. *2010 Twenty-Fifth Annual IEEE Applied Power Electronics Conference and Exposition - APEC 2010*, 01 2010.

List of Symbols, Abbreviations, and Acronyms

1-D	one-dimensional
2-D	two-dimensional
3-D	three-dimensional
Au	gold
BoP	balance-of-plant
CO ₂	carbon dioxide
DMFC	direct methanol fuel cell
EFOY	Energy for You
GaSb	gallium antimonide
Ge	germanium
H ₂ O	water
InGaAs	indium gallium arsenide
InGaAsP	indium gallium arsenide phosphide
InGaAsSb	indium gallium arsenide antimonide
InP	indium phosphide
Li	lithium
MEMS	microelectromechanical system
NASA	National Aeronautics and Space Administration
Pt	platinum
R&D	research and development
RTG	radioisotope thermoelectric generator
Si	silicon
Si ₃ N ₄	silicon nitride
TEC	thermal-to-electrical conversion

UAV

unmanned air vehicles

NO. OF COPIES	ORGANIZATION
1 ELEC	ADMNSTR DEFNS TECHL INFO CTR ATTN DTIC OCP 8725 JOHN J KINGMAN RD STE 0944 FT BELVOIR VA 22060-6218
9	US ARMY RSRCH LAB ATTN IMNE ALC HRR MAIL & RECORDS MGMT ATTN RDRL CIO LL TECHL LIB ATTN RDRL CIO LT TECHL PUB ATTN RDRL SED-E P BARNES B MORGAN I LEE B ALLMON ATTN RDRL SEE I K SABLON P UPPAL ADELPHI MD 20783-1197
1	AMC-NVESD SELMA J. MATTHEWS 10125 GRATIOT ROAD SUITE 100 FT. BELVOIR VA 22060-5816
2	CERDEC EDMUND NAWROCKI ONATHAN CRISTIANI 328 HOPKINS ROAD APG MD 21005
1	NSRDEC KAILASH SHUKLA 15 KANSAS STREET NATICK, MA 01760

INTENTIONALLY LEFT BLANK.